

Classical Emulation of Bright Quantum States

Svetlana Vlasenko, Alexander Mikhalychev, Samaneh Pakniyat, George Hanson, Amir Boag, Gregory Slepyan, and Dmitri Mogilevtsev*

The way to emulate classically a number of fundamental quantum mechanical experiments is shown, such as Hong-Ou-Mandel interference, phase measurements with NOON states and specifically structured “revivals” in Jaynes-Cummings model using coherent states with large number of photons. It is also shown that certain classes of bright non-classical states can be efficiently emulated by our technique independently of the average photon number of these states.

1. Introduction

As long as one stays within the few-photon few-mode limit and near the optical region, one can enjoy nearly complete freedom in generating, processing, and detecting photonic quantum states of the propagating field. A number of versatile methods exist to produce deterministically or conditionally such non-classical states.^[1–3] Remarkable measurement toolsets were developed for verification and exploitation of quantum properties (here one just cannot refrain from mentioning photon-number resolving photodetectors^[4–8]). However, the situation is much less optimistic when one moves to large numbers of photons. The space of states grows exponentially, and the number of ways to produce required states become rather limited. The possibility to infer quantum states suffers even more, despite remarkable recent progress in rising efficiency of tomographic procedures^[9–12] and development of such efficient ways of partial diagnostics as much-discussed “classical shadows”.^[12,13] In fact, only specific classes of bright non-classical states are available for propagating light. First of all, the Gaussian ones using the well-developed technique of three-wave mixing for producing them.^[14,15] Another class is the result of “hybridizing” of available few-photon

non-Gaussian states with multi-photon Gaussian ones (be it by simple beam-splitting of few-photon states with a bright state,^[16–18] photon adding and subtracting,^[19–21] or conditional generation from entangled Gaussian states with the help of photon-number resolving detectors^[22,23], etc.).

When one moves away from the near-optical wavelength region, the situation worsens considerably. Non-classical propagating multi-mode Gaussian states are still available by means of superconducting circuitry.^[24,25] However, even generation of propagating few-photon non-Gaussian states is challenging, as well as detection on the level of few photons (nevertheless, some remarkable progress with single-photon microwave detectors has been recently made^[26–28]).

Here, we suggest circumventing the difficulties in researching quantum effects which stem from the application of bright non-Gaussian states using an *emulation* procedure rather than actual generation of such states. In computer science, the term “emulation” stands for running a program designed for a different platform, by simulating behavior of the other system. We extend this notion to quantum states generation and detection (**Figure 1**). In a quantum experiment, the “program” describes manipulation and measurement of quantum states, while the “platform” is represented by the physical quantum systems and their particular input states. The essence of the proposed emulation technique is representation of a quantum state as a mixture of classical probe states (typically, coherent state projectors), with positive and negative weights. For emulation, the probe states are to be randomly sampled from the preconstructed set with probabilities corresponding to the normalized absolute values of the weights. Information about a particular weight sign is encoded using an additional degree of freedom (or ancillary system). Then, the compound system (i.e., signal plus ancilla) is subjected to the measurement.

The emulation procedure is constructed to ensure that the expectation values of the chosen set of observables remain the same as for the original target states (in the spirit of the “classical shadows” tomography^[12,13]). This set of observables might be a complete one suitable for the state reconstruction. In that case, one actually has to build a high-fidelity representation of the quantum signal as a mixture of classical probes with positive and negative weights. Notice that non-classicality of the original state to be emulated is actually retained by enlarging the state space.

The proposed emulation technique also resembles computational ghost imaging,^[29,30] where generation of a correlated quantum state of two beams is replaced by sampling classically modulated states of one beam and postprocessing the measurement

S. Vlasenko, A. Mikhalychev, D. Mogilevtsev
B.I. Stepanov Institute of Physics
NAS of Belarus
220072 Minsk, Belarus
E-mail: d.mogilevtsev@ifanbel.bas-net.by

S. Pakniyat, G. Hanson
Department of Electrical Engineering
University of Wisconsin-Milwaukee
Milwaukee, Wisconsin 53211, USA

A. Boag, G. Slepyan
School of Electrical Engineering
Tel Aviv University
Tel Aviv 69978, Israel

 The ORCID identification number(s) for the author(s) of this article can be found under <https://doi.org/10.1002/qute.202300060>

DOI: 10.1002/qute.202300060

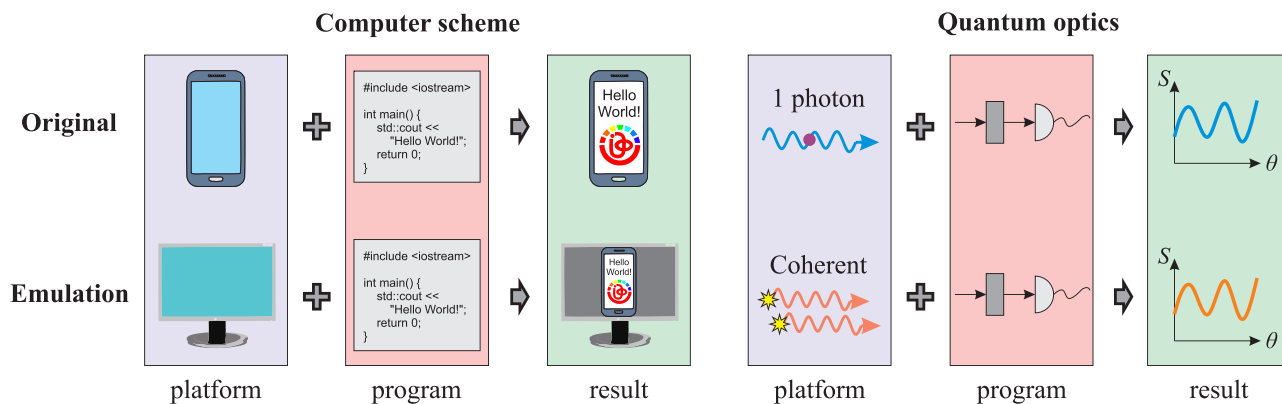


Figure 1. Generalization of the concept of emulation from computer science to quantum optics: the “platform” corresponds to input states, while the “program” is represented by measurement of quantum states.

results with the help of additionally supplied classical information about the sampled states.

The classical emulation framework can be designed prior to selecting the concrete program to be run and is suitable for any program from a particular subset. Similarly, the proposed quantum emulation can also be applied to an arbitrary “program” (state manipulation and measurement) from a certain class of states and measurements. The emulation platform remains essentially quantum (even when it is constructed from “classical” coherent probe states) and is suitable for sensing and exploring a quantum measurement setup. Also, the proposed quantum emulation procedure cannot be superseded by a classical computer simulation unless full and accurate description of the measurement setup is available, which is typically not the case for realistic quantum experiments.

Recently, we have elaborated a procedure for emulation of several fundamental quantum optical effects, namely, the Hong-Ou-Mandel (HOM) interference, non-classicality witnessing, and Bell testing with the platform of few-photon coherent states.^[31] Now, we extend the emulation technique to the platform of bright coherent states and present protocols of both “scaled” emulation of fundamental few-photon effects and representation and emulation of several important classes of bright non-Gaussian states: sub-Poissonian states (diagonal in the Fock-state basis) and the result of “hybridizing” Gaussian states with few-photon non-Gaussian states. Remarkably, while the complexity of the original protocol crucially depends on the number of photons in the target state to be emulated, our suggested extension allows one to emulate the considered classes of bright states efficiently independently of their average photon number. So, one can use our emulation approach not only for resource-economical testing and verification of measurement setups, but also for verifying quantum effects predicted for multi-photon states which are hard to produce on the current level of experimental technology. For example, one needs such sub-Poissonian non-Gaussian states for producing specific structured atomic population “revivals”^[32] in the Jaynes-Cummings scheme.^[33]

We suggest and discuss the approach of “scaled” emulation of such fundamental quantum experiments as HOM interference^[34] and interferometric phase measurement with NOON states^[35] using bright coherent states and linear power

detectors. Also, we propose an emulation scheme for observing effects of two-level atom interaction with non-Gaussian sub-Poissonian state (in particular, extension of the population revivals structure^[36,37]).

We show the feasibility of our emulation method for bright non-classical states, demonstrate its robustness with respect to noise of used coherent sources. Also, we discuss in details the way to performing HOM interference experiment by emulating single-photon inputs with sequences of randomly phased large coherent pulses amplitudes sampled from a small set of values. We describe how to choose this set in an optimal way so as to minimize the number of samples for a given accuracy level.

The outline of the paper is as follows. In Section 2, we describe essential features of the emulation method and limitations of its feasibility. In Section 3, we discuss emulation of fundamental quantum experiments (HOM scheme and phase measurement with two-photon NOON states) by “scaling” few-photon states (in particular, the single-photon one). Using linear response intensity detectors enables scaling the coherent-state amplitudes, used for representation of the non-classical state, by multiplying them by a constant factor and dividing the resulting signals by the same quantity. In Section 4 we consider production of emulated multiphoton states by unitary mixing of few-photon emulated states with bright classical ones. In Section 5 we present emulation of bright diagonal sub-Poissonian non-Gaussian states, and show that the efficiency of their representation by a few phase-averaged coherent states is independent of the average number of photons in the target state. In Section 6 we describe how to emulate effects of the atom-field interaction with sub-Poissonian states and observe extended structured revivals.

2. Essence of Emulation

Here, we briefly outline the idea of the emulation procedure described in the recent work.^[31] Let us assume that we have a signal state described by a density matrix ρ , and a set of observables $\{O_j\}$. The purpose of the emulation procedure is to reproduce the expectation values $o_j = \text{Tr}\{O_j\rho\}$ by performing similar measurements with certain easy-to-generate probe states instead of an “expensive” quantum state ρ .

According to the general formalism of quantum theory, the ability to decompose a density matrix ρ in the form^[38]

$$\rho = \sum_k p_k \rho_k \quad (1)$$

with non-negative weights $p_k \geq 0$ suggests a way to generate the state ρ . If the source produces states ρ_k with probabilities p_k , its output state will be described exactly by the target state ρ . However, it is not possible to decompose any non-classical state ρ in terms of classical states ρ_k according to Equation (1) with non-negative weights $p_k \geq 0$.^[39] Still, one can succeed in constructing an approximate representation

$$\rho \approx \rho_{\text{approx}} = \sum_k c_k^{(+)} \rho_k^{(+)} - \sum_k c_k^{(-)} \rho_k^{(-)} \quad (2)$$

where classical probe states from the subset $\{\rho_k^{(+)}\}$ are multiplied by positive factors $\{c_k^{(+)}\}$, while the remaining states $\{\rho_k^{(-)}\}$ have negative weights $\{-c_k^{(-)}\}$. Here, $\sum_k c_k^{(+)} - \sum_k c_k^{(-)} = 1$ and $c_k^{(\pm)} > 0$, $\forall k$. The signs of the coefficients cannot be captured by the probabilities of the probe states sampling by the source and require additional marking of the state by a classical bit of the sign information. Notice that very possibility of the approximate representation Equation (2) stems from non-orthogonality of used classical states $\{\rho_k^{(\pm)}\}$, which underlies a number of important applications of such states in quantum communications, for example, in developing secure quantum key distributions.^[40–43]

Physically, one can introduce an ancilla with two mutually orthogonal states $|\pm\rangle$, encoding the sign, and consider a two-system state

$$\rho_{\text{em}} = \sum_k \bar{c}_k^{(+)} \rho_k^{(+)} \otimes |+\rangle\langle +| + \sum_k \bar{c}_k^{(-)} \rho_k^{(-)} \otimes |-\rangle\langle -| \quad (3)$$

where the coefficients of the mixture

$$\bar{c}_k^{(\pm)} = c_k^{(\pm)} / C, \quad C = \sum_k c_k^{(+)} + \sum_k c_k^{(-)} \quad (4)$$

are real, positive, and sum up to unity. Since the coefficients $\bar{c}_k^{(\pm)}$ have all the properties of probabilities, the state ρ_{em} can be easily generated by sampling the states $\rho_k^{(\pm)} \otimes |\pm\rangle\langle \pm|$ with the probabilities $\bar{c}_k^{(\pm)}$.

To decode the sign, one can introduce an observable over the ancilla

$$A = C(|+\rangle\langle +| - |-\rangle\langle -|) \quad (5)$$

where the multiplier C is used for compensation of the normalization factor, which connects the coefficients $c_k^{(\pm)}$ with the corresponding probabilities $\bar{c}_k^{(\pm)}$.

The essence of the emulation is to build such a density matrix ρ_{em} that the results of measuring the joint observable $O_j \otimes A$ for the state ρ_{em} accurately reproduce the measurement of O_j for the target non-classical state ρ :

$$|o_j - \text{Tr}\{(O_j \otimes A)\rho_{\text{em}}\}| \leq \epsilon \quad (6)$$

for the acceptably small predefined ϵ .

Practically, the information carried by the orthogonal states $|\pm\rangle$ of the ancilla, is classical and can be provided to the measuring site by classical means. In that case, one should sample random pairs (k, \pm) according to the probabilities distribution $\bar{c}_k^{(\pm)}$, generate corresponding states $\rho_k^{(\pm)}$, perform the measurement of O_j , multiply the result by the normalization factor C , and sum the results with the corresponding signs \pm .^[31]

The advantage of the outlined procedure comes from the premise that the probe states $\rho_k^{(\pm)}$ are more easily generated than the signal state (for example, they may be classical Gaussian states such as coherent ones). Moreover, in some quite important cases it is sufficient to implement only a few classical probes for accurate emulating quantum effects. In particular, we have recently shown that using less than ten few-photon phase-averaged coherent states one can feasibly emulate the HOM effect, non-classicality witnessing, phase measurements with few-photon NOON states, and even Bell testing ref. [31]. Here, one has to notice that using just few-photon states^[31] actually allowed in some cases to build signal representation for a tomographically complete set of the observables O_j (to get a high-fidelity approximation of the original signal density matrix, ρ). In that case, the parameter ϵ in the bound given by inequality (6) would be limited just by this fidelity.

It should be emphasized that one can fix a set of observables $\{O_j\}$ which is not tomographically complete, and reduce the requirement $\rho \approx \rho_{\text{approx}}$ in Equation (2) to $o_j \approx \text{Tr}(O_j \rho_{\text{approx}})$. This requirement is weaker and allows more flexibility in construction of the decomposition and design of resource-efficient emulation schemes. Such schemes can provide a simple inexpensive way to test a measurement setup, developed for observation of quantum effects, which are supposed to occur due to non-classical input states.

However, in this particular work we are not seeking simplifications of the procedure described in ref. [31]. We aim at a higher-end goal. Namely, we show how it is possible to obtain high-fidelity representations of non-classical states using just a few classical ones. Such representations allow one to demonstrate fundamentally quantum effects with a large number of photons. Further, when writing about “representations” we will always have in mind high-fidelity ones.

It should be pointed out that there is a severe restriction on the way of applying the emulation procedure to arbitrary nonclassical states. The necessity to enlarge the state space and to deliver the sign information by the joint measurement of the observables O_j and A during the emulation procedure can lead to excess statistical errors relatively to the measurement of the same observable O_j with the original signal state ρ . Somewhat similar situation was encountered when simulating Bell inequalities violation by sampling the positive P-representation of the entangled states. Enlargement of the phase space led to large statistical errors.^[44,45] The addition to the variance scales as $(\sum_k c_k^{(+)}) (\sum_k c_k^{(-)})$ and can be quite large.^[31] Therefore, for practical emulation one needs to minimize this quantity. For classical signals representable as a convex mixture of classical probes one can always find a positive-weight representation with $c_k^{(-)} = 0$, $\forall k$, which yields no increase in statistical errors. Negative terms stem from the non-classicality. Representation with coherent probes is especially illustrative: one needs to have negative terms to ensure zeros of Husimi Q-function typical for non-classical states.^[46,47]

The representation of Equation (2) was developed in a series of works on the “data pattern” approach to quantum tomography.^[48–53] Mostly few-photon few-mode states were considered. In these works, it was shown that when the subspace containing the signal increases (the mean number of photons grows), the representation (2) quickly becomes unfeasible. It requires a very large number of probes, high values of coefficients $c_k^{(\pm)}$, and, correspondingly, impractically many sampled copies of probes $\rho_j^{(\pm)}$ for reaching acceptable levels of measurement accuracy.^[48–53] Also, for general signal states, the requirement of semipositive definiteness of the emulated state makes the emulation procedure cumbersome and resource-costly.^[52] While all these considerations are valid for problems requiring representation of an initially unknown quantum state with a set of predefined probes, the task of decomposing a given fixed state for its emulation was found to be much easier. Few-photon states diagonal in a Fock-state basis allow for simple and efficient emulation using several phase-averaged coherent states. Transforming these single-mode few-photon states by linear devices, such as phase-shifters and beam-splitters, one can emulate more complex states, including entangled ones.^[31]

Here, we advance these findings and describe the ways to emulate some specific non-Gaussian non-classical states with large average number of photons using efficient procedures developed primarily for few-photon states.

3. Fundamental Experiments with Scaled States

It is established that few-photon non-classical states can be efficiently approximated by sums of coherent state projectors.^[48,52] In particular, phase-averaged coherent states can be used for representing the Fock states and NOON states.^[31] Now, let us suppose that our set of observables $\{O_j\}$ contains only normally-ordered combinations of the creation and annihilation operators of the same order: $O_j \propto (a^\dagger)^n a^n$; for example, normally ordered field correlation functions $G^{(n)} \propto \langle (a^\dagger)^n a^n \rangle$. Performing those measurements for probe states with scaled amplitudes $\alpha_k \mapsto s\alpha_k$ will lead to the same scaling for all the correlation functions of the same order: $o_j \mapsto |s|^{2n_j} o_j$.

Such a scaling of the emulation procedure brings a number of practical advantages. Firstly, it allows going away from the single-photon regime and using analog detectors linear in registered intensity, that is, switching from the platform of few-photon coherent states to bright coherent states (Figure 2). Secondly, the resulting correlation functions can be normalized in such a way that the scheme becomes robust even to unknown losses as long as they only affect the scaling parameter s . Thirdly, if the representation involves phase-averaged coherent states (as it is for the decomposition of Fock states), even the interference scheme may become robust with respect to the uncorrelated phase noise.

It is worth noting that, while the emulation technique itself is quite universal, the scaled version of emulation is tailored specifically for decomposition of the target state in terms of coherent states and measurement of the discussed normally ordered correlation functions. Firstly, the scaling operation $|\alpha_k\rangle \mapsto |s\alpha_k\rangle$ is non-unitary since it does not preserve the scalar product: $\langle s\alpha|s\beta\rangle \neq \langle \alpha|\beta\rangle$ for $\alpha \neq \beta$ and $s \neq 1$. Secondly, when naively extended to probe states different from the coherent ones by scaling their

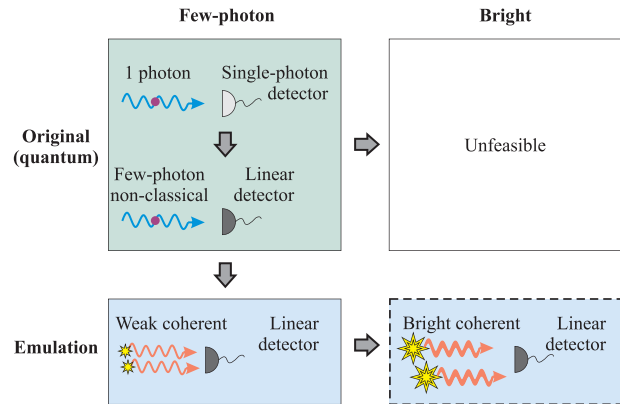


Figure 2. Exploiting the platform of bright coherent states by scaled emulation of few-photon quantum experiments. Firstly, the few-photon quantum experiment with single-photon detectors is reformulated in terms of using linear detectors. Secondly, the emulation of the few-photon experiment with linear detectors and few-photon coherent probe states is designed. Thirdly, the constructed emulation scheme is scaled in order to exploit bright coherent probe states.

Glauber-Sudarshan functions $P(\alpha) \mapsto P(\alpha/s)$, the operation can lead to nonphysical results due to violation of the non-negative semidefiniteness condition. However, the scaling approach yields accurate and physically correct results when the probe states and the measurements satisfy the conditions listed above.

Let us illustrate the possibilities of using scaled emulation technique with bright probe states on the examples of the HOM interference experiment and enhanced phase measurements with NOON states.

3.1. Hong-Ou-Mandel Interference

The famous Hong-Ou-Mandel (HOM) experiment shows that quantum interference on a 50/50 beam-splitter (BS) directs two identical input single photons to the same output of the interferometer, prohibiting the symmetric response when both single-photon detectors click simultaneously^[34] (see Figure 3(inset)).

Now, let us consider the setup, shown in the main panel of Figure 3, with single-photon detectors replaced by linear detectors, measuring the intensities I_1 and I_2 . For the j -th detector with the efficiency η , the expectation value of the measured signal I_j is described by the quantum average of the operator $\hat{I}_j = \eta \hat{n}_j$, where \hat{n}_j is the photon-number operator for the measured field mode. Due to HOM interference, the coincidence signal $\langle \hat{I}_1 \hat{I}_2 \rangle$ should be zero for interference of identical single-photon inputs.

As shown in ref. [31], a single-mode single-photon state can be represented as a mixture of phase-averaged coherent states (PACS)

$$\rho_{\text{PACS}}(x_k) = \frac{1}{2\pi} \int_0^{2\pi} d\varphi |x_k e^{-i\varphi}\rangle \langle x_k e^{-i\varphi}| \quad (7)$$

with amplitudes $x_j > 0$ and positive and negative weights c_k :

$$|1\rangle\langle 1| \approx \sum_k c_k \rho_{\text{PACS}}(x_k) \quad (8)$$

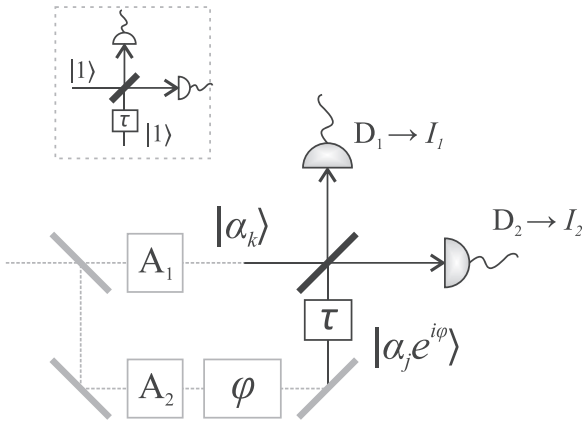


Figure 3. (Main panel) Scheme of the setup for the HOM experiment emulation with the bright scaled states. An input coherent state is split into two parts and subject to the variable losses realizing random sampling of amplitudes α_j and α_k with weights $\bar{c}_j^{(\pm)}$, $\bar{c}_k^{(\pm)}$ as described in the Section 2. Then a random phase shift φ is applied in one of the arms. Afterwards, resulting states interfere on the 50/50 BS and the signals are measured by the intensity detectors. Inset shows a standard HOM interference scheme with single-photon states at the BS inputs and single-photon detectors at the outputs. The element “ τ ” in both schemes represents an optical delay line which realizes the time delay τ between two arms of each scheme.

Therefore, the two-mode two-photon input of the interferometer has the representation

$$|1, 1\rangle\langle 1, 1| \approx \sum_{j,k} c_j c_k \rho_{\text{PCS}}^{(1)}(x_j) \otimes \rho_{\text{PCS}}^{(2)}(x_k) \quad (9)$$

where $\rho_{\text{PCS}}^{(l)}(x_k)$ denotes the k -th PCS Equation (7) of the l -th input mode. As it was pointed out in ref. [31], accurate representation of the input states can be built with just a few distinct amplitudes of PCSs, while a single laser source and a variable BS are sufficient for emulation of the HOM experiment. The scaling procedure implies change of the PCSs’ amplitudes according to the rule $\rho_{\text{PCS}}^{(l)}(x_k) \mapsto \rho_{\text{PCS}}^{(l)}(sx_k)$.

Let us show how such a scheme shown in Figure 3 is functioning. An input coherent pulse is split in two parts and subject to the variable losses realizing random sampling of amplitudes $s\alpha_j$ and $s\alpha_k$ with the weights $\bar{c}_j^{(\pm)}$, $\bar{c}_k^{(\pm)}$ as described in the Section 2. Then, a random phase shift φ is applied in one of the arms producing phase averaging necessary for our single-photon states’ representation. Afterwards, the resulting states interfere on a 50/50 BS, with the outcome being recorded by the intensity detectors. We assume measurement of the intensities $I_1 = \langle \hat{I}_1 \rangle$ and $I_2 = \langle \hat{I}_2 \rangle$ together with the coincidence signal

$$C_{12} = \langle \hat{I}_1 \hat{I}_2 \rangle = \frac{\eta^2}{4} \langle (|a_1^\dagger|^2 + |a_2^\dagger|^2)(a_1^2 + a_2^2) \rangle \quad (10)$$

where a_j , a_j^\dagger are the annihilation and creation operators of the j -th input mode. The results for a particular sampled pair of amplitudes are assigned the sign of the product $c_j c_k$ and multiplied by the factor C , defined in Equation (4). The estimates for expectation values of the measured quantities are formed by summing

the collected results for the sampled states and dividing them by the total number of samples N :

$$\langle \hat{X} \rangle \approx \sum_{m=1}^N X_m / N \quad (11)$$

where the operator \hat{X} stands for the measured quantities \hat{I}_1 , \hat{I}_2 , and $\hat{I}_1 \hat{I}_2$; X_m is the measurement result for the quantity \hat{X} and the m -th sampled state. In the limit of a large number of samples, this procedure accurately reproduces the expectation values of the measured quantities for the target state ρ up to the scaling multiplier s^2 for the intensities I_1 and I_2 and s^4 for the coincidence signal C_{12} . It is straightforward to see that if the state Equation (9) turns the average value $\langle \hat{I}_1 \hat{I}_2 \rangle$ to zero, then for any s this average is also zero. Therefore, scaling does not spoil the HOM interference effect.

Usually, the HOM interference is demonstrated through the so-called “Hong-Ou-Mandel dip”, when one makes the interference of pulses imperfect and shows how the probability of simultaneous counts on both detectors increases for growing degree of imperfection. This is usually demonstrated by measuring the normalized intensity correlation function

$$\tilde{g}_2 = \frac{\langle \hat{I}_1 \hat{I}_2 \rangle}{\langle \hat{I}_1 \rangle \langle \hat{I}_2 \rangle} \quad (12)$$

For the discussed scaled emulation technique, both the numerator and the denominator of the expression scale as s^4 , thus ensuring independence of \tilde{g}_2 of the scaling parameter s (up to statistical noise, which decreases for larger s).

One can make the interference imperfect, for example, by adding a delay in one of the interferometer arms to make the pulses partially overlapping on the 50/50 BS. We discuss a realization of the Hong-Ou-Mandel interference scheme in Supplement A. In particular, it is shown that if the extent of the pulses’ overlap is f (e.g., for rectangular pulses of duration T and relative delay τ , this quantity equals $f = |T - \tau|/T$ for $\tau \in [0, T]$ and $f = 0$ otherwise), one has $\tilde{g}_2 \approx (1 - f)/2$. The results of numerical modeling are shown in Figure 4. The plotted correlation function is re-normalized by its value $\tilde{g}_2 = 0.5$ for non-overlapping ideal single photons.

Notably, as it was discussed for single-photon emulation of the Hong-Ou-Mandel interference in ref. [31] and was mentioned in Section 2, suboptimal representation of the single-photon state can lead to large statistical errors and, consequently, to large number of measurement runs necessary for demonstrating the Hong-Ou-Mandel interference. In the Supplement B, we discuss the optimization of the single-photon state representation using PCSs. One can see from the results presented in Figure 4 that using just four bright PCSs, one can reach $2\tilde{g}_2 \lesssim 0.05$ for the completely overlapping pulses for just 10^7 measurement runs. Notice that using just coherent states with independently randomly fluctuating phases without the emulation procedure, one always has $2\tilde{g}_2 \geq 0.5$.^[54]

It is also worth noting that our HOM emulation procedure can be easily realized not only in the optical region, but also with microwaves, where intensity detectors with linear response are easily available. In contrast to the optical wavelength region, the mi-

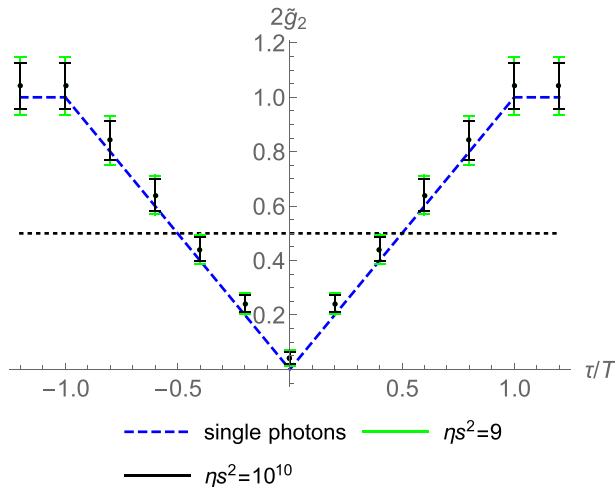


Figure 4. Dependence of the re-normalized second-order correlation function $2\tilde{g}_2(\theta)$ on the normalized relative shift τ/T of rectangular pulses with the duration T . Solid lines indicate the dependence for interference of two single-photon states. Points and error bars show the values and the standard deviations for scaled emulation of single-photon states for $N = 10^7$ repetitions and effective scaling of photon number $\eta s^2 = 9$ (green) and 10^{10} (black). Dashed line shows the maximal depth of the HOM dip for the interference of classical states.

crowave HOM experiment was performed only quite recently.^[55] There, generation of microwave single photons was achieved by independent superconducting circuits. Due to the absence of adequate single-photon detectors, heterodyne detection at the outputs of the HOM beam-splitter was used with long trains of single-photon pulses to measure the second-order correlation functions.^[56]

Finally, it is worth noting that one can develop the representation (7) using not only PCSs, but any kind of classical states, even thermal ones.^[48,49,57] Notice that just two thermal states are sufficient for representing a single-photon state;^[49] also, the density operator of a heralded single photon produced from an unentangled photon pair is exactly a difference of two thermal states.^[57] In order to make the microwave HOM emulation more feasible, noisy coherent states can also be used (Supplement B).

3.2. Phase Estimation

Another quantum experiment feasible for emulation with scaled bright coherent states is phase estimation with two-mode NOON states,

$$|\psi\rangle = \frac{1}{\sqrt{2}}(|n\rangle_1|0\rangle_2 + |0\rangle_1|n\rangle_2) \quad (13)$$

Introducing a phase shift θ for the first mode adds the n -times enhanced phase factor $e^{in\theta}$ to the first term of Equation (13), which can be extracted by an interferometric measurement of the observable $R_n = |n\rangle_1|0\rangle_2\langle 0|_1\langle n|_2 + |0\rangle_1|n\rangle_2\langle n|_1\langle 0|_2$.^[35] The dependence $\langle R_n \rangle = \cos(n\theta)$ yields favourable scaling of the precision of the phase shift estimation with the number of photons n and enables reaching Heisenberg limit of quantum measurement precision.^[58,59] It is remarkable that one does not need to build an

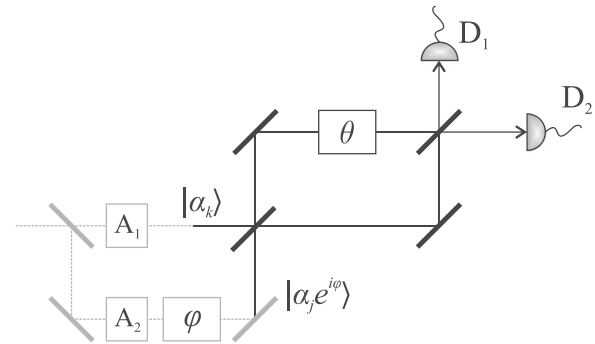


Figure 5. Scheme of interferometer for emulation of the experiment for phase estimation with bright scaled states. Emulated bright single-photon states are generated as for Figure 3. Then, they are mixed at 50/50 BS and inputted into the interferometer. Its outputs are measured by the intensity detectors $D_{1,2}$. The phase shift θ is to be estimated.

involved scheme suitable for measurement of the observable R_n . It is sufficient to register n photons in the symmetric compound mode $a_1 + a_2$, (i.e., to detect the n -photon state after mixing the modes at a symmetric beam splitter), since the probability of the event is proportional to $1 + \langle R_n \rangle$ for the considered state.^[60]

In our previous work,^[31] we have demonstrated the way to develop simple and feasible representations of few-photon NOON states. So, using the scaled emulation procedure for these states and performing measurement of the n th-order correlation function of the symmetric compound mode with intensity detectors, it is possible to emulate the phase measurement with NOON states.

As an example, let us demonstrate how it can be done for $n = 2$. For that purpose, one needs only a simple modification of the scheme shown in Figure 3 with two input emulated single-photon states. This modified scheme is shown in Figure 5. Scaled emulation of single-photon states is performed in the same way as in the previous subsection. The signal enters the interferometer with the phase shift θ in one of the arms through the 50/50 BS. Then, the outputs are measured by the intensity detectors and the normalized second-order cross-correlation function (12) is estimated. In Figure 6, the results of the phase shift θ estimation are shown for optimal representation of the single-photon state used in the previous subsection. The errors bars are shown for $N = 10^7$ measurement runs. In Supplement C, we discuss details of the emulation.

It is to be noticed that the scheme of Figure 5 can also be easily accommodated for an experiment in the microwave region similarly to the HOM emulation scheme.

4. “Hybridizing” States

An obvious way of producing bright non-classical states is to hybridize available few-photon states with bright classical states transferring non-classical features of a few-photon state to the bright one. The scheme of the hybridizing few-photon states with bright states and its emulation is shown in Figure 7. As an example, one can consider mixing a single-photon state $|1\rangle$ with a

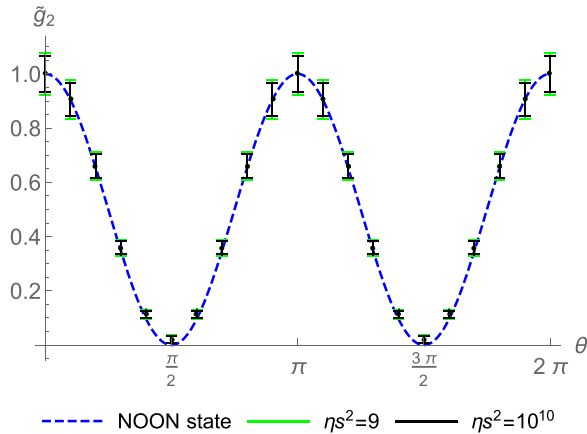


Figure 6. Dependence of the normalized second-order correlation function $\tilde{g}_2(\theta)$ on the measured phase shift θ . Solid lines indicate the dependence for the original 2-photon NOON-state. Points and error bars show the values and the standard deviations for scaled emulation of single-photon states for $N = 10^7$ repetitions and effective scaling of photon number $\eta s^2 = 9$ (green) and 10^{10} (black).

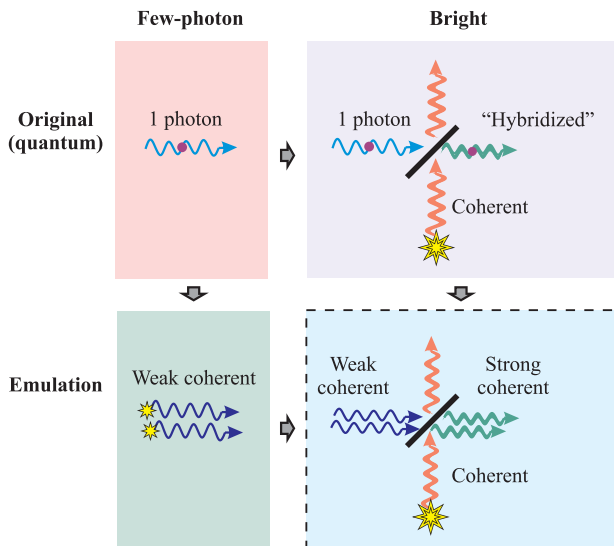


Figure 7. Exploiting the platform of bright coherent states by emulation of “hybridized” states. Firstly, non-classical features of a few-photon state are transferred to a bright state by considering its “hybridization”. Secondly, an experiment with the “hybridized” state is emulated using bright coherent probe states. The representation of the target “hybridized” state can be found by constructing the decomposition of the few-photon state and “hybridizing” each of the probe states. For coherent probes, “hybridization” means just a displacement of the state amplitude.

bright coherent state at a BS. The result of such “hybridization” is described by the coherent shift:

$$|1\rangle(\beta) = D(\beta)|1\rangle, \quad D(\beta) = \exp\{\beta(a^\dagger - a)\} \quad (14)$$

where for the sake of simplicity the amplitude β is taken to be real. For large $\beta \gg 1$, the resulting state $|1\rangle(\beta)$ is bright (its mean photon number equals $\beta^2 + 1$) and retains non-classical features (the Glauber function of the “hybridized” $|1\rangle(\beta)$ and the original $|1\rangle$ states differ by a translation in the phase space only).

Other schemes of “hybridization” by BS mixing, coherent shifting and photon adding^[3,16–21] have already been mentioned above in the Introduction.

Naturally, one can use these schemes also to produce emulated bright non-classical states using emulated few-photon states. Suppose that a few-photon non-classical state $\rho = |\psi\rangle\langle\psi|$ can be represented in terms of coherent states projectors with the amplitudes α_k . Then, the state, “hybridized” by coherent shift, has an obvious decomposition with the same number of probe states, the same values of their weights, and linearly displaced amplitudes:

$$\rho(\beta) = D(\beta)\rho D^\dagger(\beta) \approx \sum_k c_k |\alpha_k + \beta\rangle\langle\alpha_k + \beta| \quad (15)$$

One might even expect “hybridizing” to be simpler and more robust with respect to losses because of the classicality of states used for emulation.

Since ideal “hybridization” is described by a unitary transformation, it does not alter the emulation fidelity. Moreover, it preserves the upper bound^[31] of the systematic error for emulation of measuring observables with bounded spectrum of eigenvalues ($|\lambda_k| \leq M$ for all k and certain fixed $M > 0$). For example, this statement holds for measuring probabilities of certain detection events. On the other hand, an increase in the statistical errors of emulated states discussed in Section 2 clearly hints at possible problems with noise when “hybridizing” emulated states, especially for observables with unbounded spectra and mean values scaling with the growth of the mean photon number (for example, field quadratures). The influence of “hybridizing” on the statistical errors can be easily estimated from the general result obtained in our previous work.^[31] The difference between the variance $\Delta_{\text{true}} O$ of an observable O for the original quantum “hybridized” state and the variance $\Delta_{\text{em}} O$ calculated for the observable $O \otimes A$ and the corresponding emulated state ρ_{em} equals

$$\Delta_{\text{em}} O - \Delta_{\text{true}} O = 4\zeta_+ \zeta_- (\text{Tr}\{\hat{\rho} O^2\}) \quad (16)$$

where $\zeta_{\pm} = (\sum_k c_k^{(\pm)})$ and the density matrix

$$\hat{\rho} = \sum_k \frac{c_k^{(+)}}{2\zeta_+} \rho_k^{(+)} + \sum_k \frac{c_k^{(-)}}{2\zeta_-} \rho_k^{(-)} \quad (17)$$

Equation (16) shows that when $\langle O^2 \rangle$ increases with the mean number of photons in the state, one might need significantly more measurement runs for accurate estimation of O with the emulated “hybridized” state than with the original emulated few-photon state.

Now, let us show how emulation affects the influence of noise of a bright classical state used for “hybridizing” on the example of a simple coherent displacement. Influence of the amplitude noise, unavoidable in a realistic experiment, leads to the following state

$$\rho'(\beta) = \mathcal{E}(\rho(\beta)) \quad (18)$$

where

$$\mathcal{E}(\rho(\beta)) = \int d^2\epsilon p(\epsilon) D(\beta\epsilon)\rho D^\dagger(\beta\epsilon) \quad (19)$$

is the completely positive trace-preserving quantum operation induced by the complex-valued relative amplitude noise ϵ with the probability distribution $p(\epsilon)$. For Gaussian noise with the standard deviation σ , one has the following expression for the fidelity of the noised state $\rho'(\beta)$ relatively to the ideal target state $\rho(\beta)$:

$$F = \frac{1}{2\pi\sigma^2} \int d^2\epsilon \exp\{-|\epsilon|^2/(2\sigma^2)\} |\langle \psi | D(\epsilon\beta) | \psi \rangle|^2 \quad (20)$$

In the limit $\beta^2\sigma^2 \ll 1$, Equation (20) leads to the following scaling of infidelity

$$1 - F \approx 2\beta^2\sigma^2 (\langle a^\dagger a \rangle + \langle aa^\dagger \rangle - 2\langle a^\dagger \rangle \langle a \rangle) \quad (21)$$

where the averaging is performed over the original state $|\psi\rangle$. Equation (21) confirms the intuition that large coherent displacement ($\beta \gg 1$) of non-classical states requires highly stable displacing fields (the acceptable relative noise has to be small: $\sigma \ll 1/\beta$).

It is worth noting that the noise of the classical states used for “hybridizing” can mitigate imperfections of few-photon state emulation. According to the general properties of completely positive trace-preserving maps,^[61,62] the overlap between the noisy states $\rho'(\beta)$ and $\mathcal{E}(D(\beta)\rho_{\text{approx}}D^\dagger(\beta))$ is larger than or equal to the initial overlap between the original few-photon state $\rho = |\psi\rangle\langle\psi|$ and its representation ρ_{approx} :

$$F(\rho'(\beta), \mathcal{E}(D(\beta)\rho_{\text{approx}}D^\dagger(\beta))) \geq F(\rho, \rho_{\text{approx}}) \quad (22)$$

To conclude, the discussed emulation of “hybridized” states clearly indicates the ability of genuine emulation of certain bright non-classical states without specific assumptions, which are required for scaled emulation presented in the previous section. On the other hand, both the original “hybridized” states and their emulation are vulnerable to noise of the bright classical states used for the “hybridization”. Therefore, for practical applications, it is more advantageous to consider inherently bright non-classical states and to construct their decomposition directly without exploiting known representations of few-photon states.

5. Emulating Bright Diagonal States

Here, we discuss a quite wide class of non-classical states that can be efficiently emulated by virtue of being bright and without any analogies in the few-photon region. The key to this approach is the possibility to approximate a photon-number distribution of the true state, ρ_{nn} , by a linear envelope of photon number distributions, $\rho_{nn}^{(k)}$, of easily produced classical states

$$\rho_{nn} \approx \sum_k c_k \rho_{nn}^{(k)}, \quad \forall n \quad (23)$$

where the real coefficients c_k can be negative. This representation ensures accurate emulation of the measurement results for the observables $\{O_j\}$ and the state ρ , if this ρ or all the observables $\{O_j\}$ are diagonal in the Fock states basis.

The problem of the fitting (23) can be greatly simplified for bright states with smooth photon-number distributions, when

one can treat n as a continuous variable, that is, when it is possible to introduce a smooth photon-number distribution functions $\rho_{nn} \rightarrow p(n)$ and $\rho_{nn}^{(k)} \rightarrow p_k(n)$ satisfying

$$\sum_{n=0}^{\infty} |p(n) - \rho_{nn}| < \epsilon, \quad \sum_{n=0}^{\infty} |p_k(n) - \rho_{nn}^{(k)}| < \epsilon, \quad \forall k \quad (24)$$

for acceptably small ϵ .

A typical example of such states are coherent ones (including PCSs). For them, in the limit of a large average number of photons, $\langle n \rangle \gg 1$, it is possible to approximate their Poissonian distribution of the photon numbers with the Gaussian function:^[63]

$$p_k(n) = \frac{1}{\sqrt{2\pi}|\alpha_k|} \exp\left\{-\frac{(n - |\alpha_k|^2)^2}{2|\alpha_k|^2}\right\} \quad (25)$$

where α_k is the amplitude of the k -th coherent probe state.

Let us show how one can develop a fitting procedure using the representation Equation (23) with the help of bright PCSs with photon-number distributions described by Equation (25).

An important and practically relevant class of bright sub-Poissonian states also possesses the discussed smoothness of the photon number distribution, which can be continuously approximated in the following way:

$$p_Q(n) = \frac{1}{\sqrt{2\pi(Q+1)n_Q}} \exp\left\{-\frac{(n - n_Q)^2}{2(Q+1)n_Q}\right\} \quad (26)$$

where n_Q is an average photon number of the considered non-classical state, and Q is the Mandel parameter describing photon-number squeezing. It is defined as^[64]

$$Q = \frac{\Delta n^2}{n_Q} - 1 \quad (27)$$

where Δn^2 is the variance of the photon number distribution in Equation (26). Negative values of Q correspond to non-classicality, that is, to the states (26) with the photon number-distribution narrower than for the coherent state with the same average number of photons, $|\alpha|^2 = n_Q$. The state of Equation (26) is considered in the next Section as the one producing a specific kind of “revivals” of atomic population in Jaynes-Cummings model.^[33]

5.1. Direct Fitting

Now, let us demonstrate that one can actually develop a scalable representation Equation (23) for the sub-Poissonian state Equation (26) in terms of the states Equation (25) with the fidelity independent of n_Q . The problem Equation (23) of finding the real-valued decomposition coefficients c_k and the absolute values $|\alpha_k|$ of the probe coherent states’ amplitudes α_k for the case can be recast as a problem of minimizing the distance

$$D = \int_{-\infty}^{+\infty} dx \left[p_Q(x) - \sum_k c_k p_k(x) \right]^2 \quad (28)$$

where $p_k(x)$ is defined according to Equation (25) for the probe state with the amplitude α_k . Additionally, to provide the non-negativity of the representation, the following constraint should be imposed:

$$\sum_j c_j p_j(n) \geq 0 \quad (29)$$

together with the unity of the trace, $\sum_j c_j = 1$.

Generally, the condition (29) should hold for all n . In practice, one might look for its fulfillment for $n \in [n_{\min}, n_{\max}]$, such that $|n_Q - n_{\min, \max}| \gg \sqrt{n_Q}$. Positivity outside this region can be ensured by requiring positivity of the coefficients c_k corresponding to the maximal and minimal absolute values of the chosen probe state amplitudes, $|\alpha_k|$.

Let us define the following normalized quantities

$$\varepsilon = \frac{n - n_Q}{\sqrt{n_Q}}, \quad \varepsilon_k = \frac{|\alpha_k|^2 - n_Q}{\sqrt{n_Q}} \quad (30)$$

Then, according to the expressions (25) and (26), the normalized deviation of the photon number ε is distributed according to the probability densities

$$f(\varepsilon) = \frac{1}{\sqrt{2\pi(Q+1)}} \exp\left\{-\frac{\varepsilon^2}{2(Q+1)}\right\} \quad (31)$$

and

$$f_k(\varepsilon) = \frac{1}{\sqrt{2\pi}} \exp\left\{-\frac{(\varepsilon - \varepsilon_k)^2}{2}\right\} \quad (32)$$

for the sub-Poissonian state and the coherent probe states, respectively.

Now, let us assume that our probes do not differ much in intensity from the target, such that $\varepsilon_k \sim 1$. Then the distance given by Equation (28) reduces to

$$D \approx \frac{1}{\sqrt{n_Q}} \int_{-\infty}^{+\infty} d\varepsilon \left[f(\varepsilon) - \sum_j c_j f_j(\varepsilon) \right]^2 \quad (33)$$

The average number of photons, n_Q goes into Equation (33) as a multiplier. So, the optimization procedure for the coefficients $\{c_j\}$ and the normalized photon-number of the probe states, $\{\varepsilon_j\}$ does not depend on n_Q .

Substituting the expressions (31) and (32) into Equation (33), we arrive at the following quadratic form for the distance

$$2\sqrt{\pi n_Q} D = \frac{1}{\sqrt{(1+Q)}} - \sum_j b_j c_j + \sum_{j,k} c_j A_{jk} c_k \quad (34)$$

where

$$b_j = \frac{2}{\sqrt{(1+Q/2)}} \exp\left\{-\frac{\varepsilon_j^2}{4(1+Q/2)}\right\} \quad (35)$$

$$A_{jk} = \exp\left\{-\frac{(\varepsilon_j - \varepsilon_k)^2}{4}\right\} \quad (36)$$

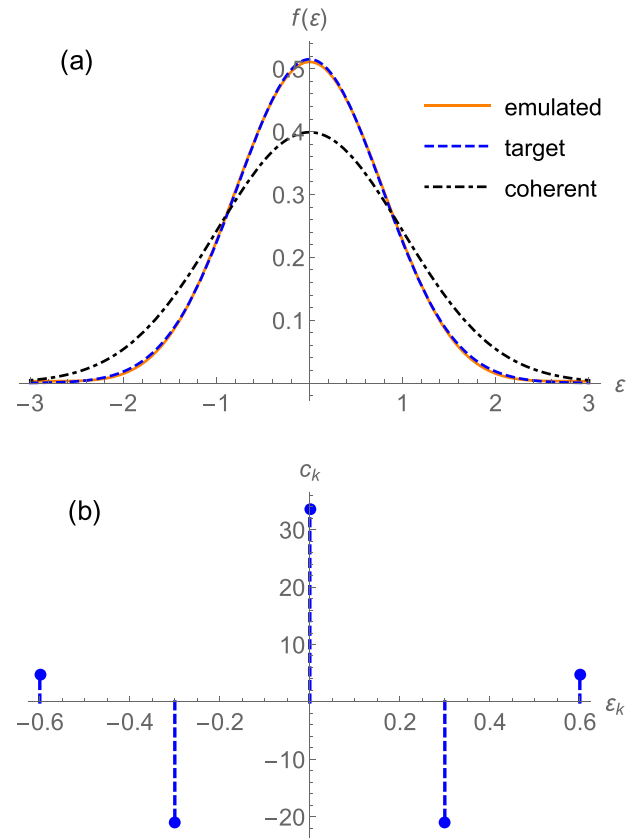


Figure 8. Representation of a sub-Poissonian state with $Q = -0.4$ as a mixture of 5 PCSs with positive and negative weights. (a) Distribution of the normalized deviation ε (Equation (30)) of the photon-number distribution of emulated (solid orange line), target (sub-Poissonian, dashed blue line), and coherent (dot-dashed black line) states for the average photon number $n_Q \gg 1$. The decomposition was constructed for minimization of the distance (34) by optimizing the PCSs parameters ε_k and the coefficients c_k of the representation (23). The parameters of the optimal decomposition are shown in panel (b).

Figure 8 shows the decomposition of a sub-Poissonian state Equation (26) with $Q = -0.4$ and the number of photons $n_Q \gg 1$ in terms of PCSs by minimization of the distance (34). One can see that the photon-number squeezed state is quite precisely emulated with only a few phase-averaged coherent probes.

Obviously, the procedure described here can be easily generalized for an arbitrary smooth photon number distribution. This procedure will provide the emulation independent on the average number of photons, on condition that the widths of the target state and the probe states scale in the same way (for example, as $\Delta n \propto \sqrt{\langle n \rangle}$ for coherent states and a sub-Poissonian state with fixed Q as discussed above).

5.2. Reverse Fitting

Generally, the procedure described in the previous subsection starts from a particular kind of a sub-Poissonian state (26) and includes optimization of the coefficients c_k to develop a representation of this target state. The set of the probe PCSs can be either fixed or optimized simultaneously with the decomposition coef-

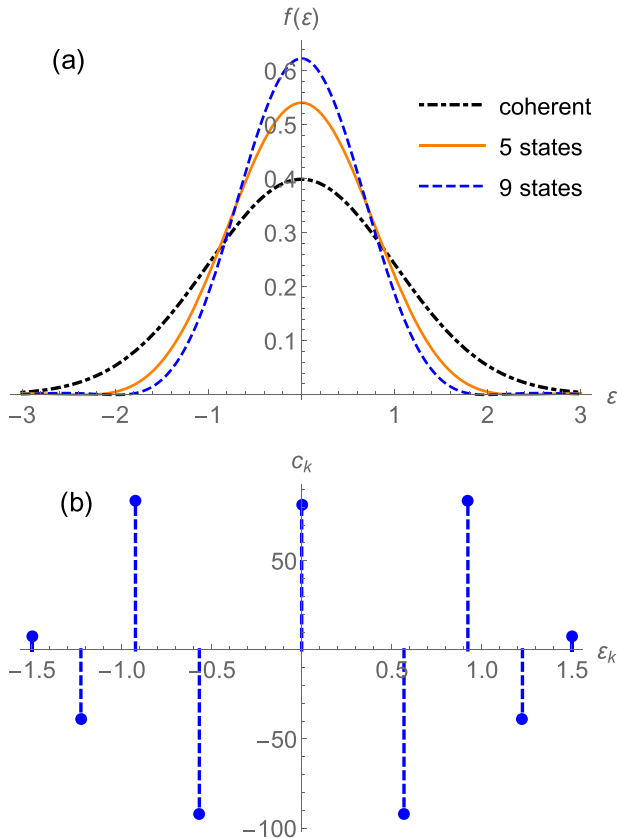


Figure 9. Examples of the reverse-fitted distribution obtained by minimization of Q -parameter (37) for different number K of the probes. Both, the PCSs parameters ϵ_k and the coefficients c_k of the representation (23) were optimized. (a) Dot-dashed black, solid orange, and dashed blue lines show the normalized deviation of the photon number distribution for the number of probe states $K = 1$ (single PCS with Poissonian distribution), 5 (Mandel parameter reaches the value $Q = -0.44$), and 9 ($Q = -0.58$). (b) Optimal representation of the sub-Poissonian state by $K = 9$ probe PCSs.

coefficients c_k . However, the procedure can be reversed and put in the following way: provided we have a fixed number K of PCS probes, what is the minimal Q of a state with a smooth photon number distribution that we can emulate using this set of probes?

Using Equations (27) and (30), the Mandel parameter can be expressed as

$$Q = \sum_{k=1}^K c_k \epsilon_k^2 - \left(\sum_{k=1}^K c_k \epsilon_k \right)^2 \quad (37)$$

Instead of choosing a specific sub-Poissonian state and searching for its decomposition in terms of PCSs, one can directly minimize the value of Q conditioned by Equation (29).

Figure 9 shows the examples of such a reverse fitting for the probes numbers $K = 5$ (solid blue line) and 9 (dashed red line). For comparison, the black dot-dashed line in panel (a) shows the photon number distribution for the PCS ($K = 1$). An example of the optimal coefficients c_k describing the contribution of each PCS and the optimal parameters ϵ_k is shown for $K = 9$ in Figure 9b. The results indicate the possibility to reach larger photon-number squeezing by relaxing the requirement for the

state to possess the fixed shape (26) of the photon number distribution.

6. Emulation of “Collapses” and “Revivals”

Here, we show that the emulated bright non-classical states described in the previous section can be used for demonstrating quantum effects that are not feasible with the few-photon states. Namely, these are specific quantum “collapses” and “revivals” in population dynamics of a two-level system interacting with a single quantum field mode.

More than forty years ago, it was discovered that in the Jaynes-Cummings model^[33] of a two-level system interacting with a single quantum field mode, initial coherent state of this mode with sufficiently large average number of photons leads to periodic “collapses” and “revivals” of the atomic population.^[36] This finding attracted a considerable interest in this phenomenon, both theoretical and experimental. First experimental observation is dated as far back as 1987 with a single-atom maser.^[65] The Jaynes-Cummings model gave rise to a plethora of important theoretical predictions and experimental observations, such as, for example, Rabi splitting,^[66–68] antibunching and sub-Poissonian statistics of the intra-cavity field,^[69,70] phase and amplitude bistability,^[71,72] a variable source for conditional and unconditional generation of non-classical states.^[73–77]

However, up to this date there are no experiments demonstrating “collapses” and “revivals” due to atomic interaction with a single-mode field in a non-Gaussian non-classical state. In particular, specific “structured revivals” were predicted for the initial state given by Equation (26). If the mode is prepared in a coherent state, the “collapses” and “revivals” lose their periodic well-structured character during the system evolution and reduce to noise-like oscillations. Photon-number squeezing with the initial state (26) extends the region of regular structure of “collapses” and “revivals”. But this prediction was not verified due to difficulties in generation of such states. Here, we demonstrate the feasibility of reproducing such “collapses” and “revivals” using emulated sub-Poissonian states with a Gaussian photon-number distribution Equation (26).

The Jaynes-Cummings system consists of a two-level atom (TLA) interacting with a single quantized field mode a . For the resonant case, in the rotating-wave approximation and in the frame rotating with the atomic transition/modal frequency, this system is described by the following interaction Hamiltonian

$$H = \hbar\Omega(\sigma^+ a + a^\dagger \sigma^-) \quad (38)$$

where the atomic raising and lowering operators are $\sigma^\pm = |\pm\rangle\langle\mp|$, the vectors $|\pm\rangle$ denote upper and lower atomic levels; the parameter Ω is the Rabi frequency describing strength of the atom-field coupling.

For the atom initially in the lower state $|-\rangle$, there is a simple solution (see Supplement D) for the time-dependent upper-state atomic population:^[33]

$$P(t) = \sum_{n=0}^{\infty} p(n) \sin^2 \left[\frac{\Omega\sqrt{nt}}{2} \right] \quad (39)$$

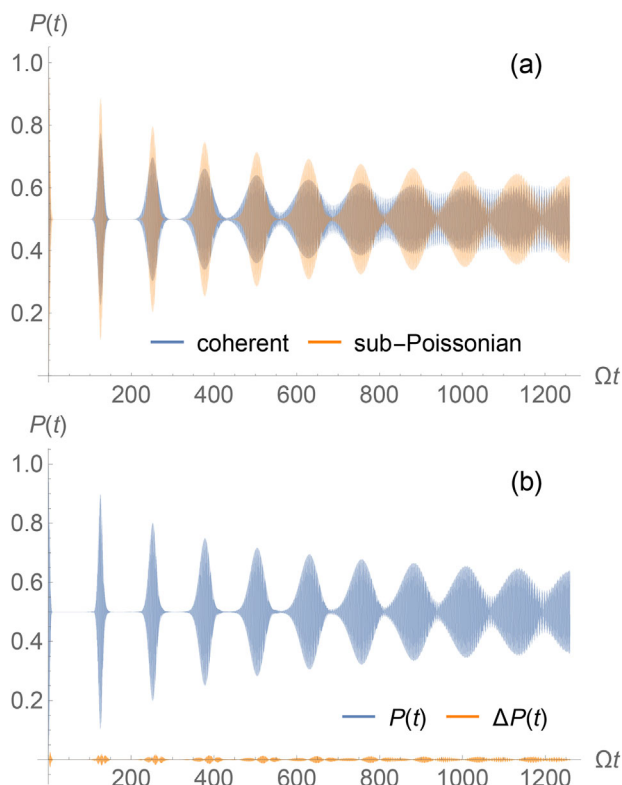


Figure 10. Effect of “Collapses” and “revivals” for small time scale: (a) for a coherent (blue line) and target sub-Poissonian (orange line) initial state (26); (b) for an emulated sub-Poissonian state (blue line). The lower orange line in panel (b) shows the difference $\Delta P(t)$ between the upper-state atomic population $P(t)$ for the emulated and the target sub-Poissonian states. The average photon number is $\langle n \rangle = 100$ for all shown states. The Mandel parameter is $Q = -0.58$ for the sub-Poissonian states. The 9-state representation (Figure 9) of the sub-Poissonian state was used for the emulation.

$p(n)$ being a photon-number distribution of the true initial state of the mode a . For the mode prepared in a Fock state, the solution (39) describes just harmonic oscillations of the atomic population. The same behaviour would occur for the coherent initial state with a large amplitude, $|\alpha| \rightarrow \infty$. Obviously, for narrow photon-number distributions (which is typical, for example, for the small average number of photons of the mode a) only a few harmonic components would contribute to the sum (39). But surprisingly it appears that when the number of photons increases to mesoscopic values, the atomic population (39) exhibits regular intermittent pattern of “collapses” and “revivals” around the equal population of excited and ground levels.^[36] The solid blue line in **Figure 10a** illustrates this phenomenon for the initial coherent state of the field mode. One can see that after a few well-separated regular “collapses” and “revivals” the atomic population oscillates in a noise-like manner. Intervals between the “revivals” disappear. Photon-number squeezing allows one to extend the region of the structured well-separated “collapses” and “revivals” changing respective widths and heights of the “revival” oscillations as well. In **Figure 10b**, it is shown that the emulation with quite a modest number of phase-averaged coherent probes (see Supplement D for details) allows one to reproduce very precisely an extension of

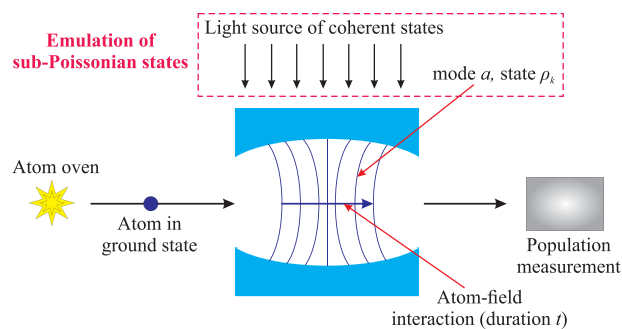


Figure 11. Scheme of a setup suitable for emulation of “collapses” and “revivals” in Jaynes-Cummings model. Two-level atoms, initialized in the ground state, pass through a single-mode cavity and then are subjected to the population measurement. Varying the speed of the atoms, one can control the duration t of the atom-field interaction preceding the measurement. Before passage of each atom, the field mode is excited to a PCS ρ_k , sampled according to the representation (23).

the structured “collapses” and “revivals” dynamics region typical for true photon-number squeezed states (26). For the representation used to obtain **Figure 10b**, 9 states were used. The average photon number of the emulated state is 100, Mandel parameter $Q = -0.58$; the coefficients c_k and the normalized amplitudes ϵ_k are shown in **Figure 9b**.

Figure 11 shows a scheme suitable for emulation of “collapses” and “revivals” employing a setup similar to the one used in ref. [65]. Two-level atoms, initialized in the ground state, pass through a single-mode cavity, where the sub-Poissonian state is emulated, and then are subjected to the population measurement. Repeating the experiment with different duration t of the atom-field interaction (the time needed for an atom to pass through the cavity), one can measure the dependence of the upper-state atomic population $P(t)$ on the dimensionless parameter Ωt , shown in **Figure 10**.

7. Conclusions

In this work, we have shown how to extend the emulation of non-classical states suggested in the previous work^[31] toward the platform of multi-photon bright coherent states. Direct approaches to this problem, based on extension of known decompositions of few-photon non-classical to a larger number of photons, quickly became unfeasible with the increase of the average number of photons of the state to be emulated. One needs too many probes. Correspondingly, one faces too large statistical errors when trying to emulate results of quantum experiments. We have suggested three different approaches for overcoming this problem. Firstly, we have developed a scaling procedure for emulation of the few-photon states for demonstrating such fundamental experiments as Hong-Ou-Mandel interference and phase estimation with NOON states. The essence of this approach is to scale similarly amplitudes of all the coherent probes so as to obtain the same normalized normally-ordered correlation functions as for the original few-photon state. We have demonstrated practical feasibility of the Hong-Ou-Mandel interference experiment with emulated scaled single-photon states using just four probes.

Secondly, we have demonstrated that one can emulate “hybridizing” bright classical states with few-photon non-classical

states by modifying the probe coherent states accordingly. For example, one can coherently displace few-photon emulated non-classical states, add or subtract a single-photon emulated state, etc. Noise of the bright classical state can even improve fidelity of the “hybridization” with the emulated state in comparison with the true one. However, it is better to optimize emulation with respect to the statistical errors propagation for the “hybridized” state and not the original few-photon one.

Thirdly, we demonstrated that it is possible to emulate efficiently bright non-classical states, diagonal in the Fock states’ basis, with smooth localized photon number-distributions in such a way that the emulation procedure does not depend on the average photon number of the target state. We have shown that such emulation opens the way for experimental observation of effects that were not available due to impossibility to generate multi-photon non-classical states required for this. As an example, we have shown how one can observe structured “collapses” and “revivals” in the Jaynes-Cummings model with photon-number squeezed multi-photon states.

In conclusion, the developed procedures for non-classical emulation of bright states open wide possibilities for testing experimental setups and observing effects that were otherwise unfeasible due to problems with generating non-classical states.

Appendix A: Scaled Emulation of Hong-Ou-Mandel Effect

Figure A1 shows a 4-mode representation of the HOM measurement with partially overlapping modes. The original 2-photon state with the overlap f can be represented as

$$|1, 1\rangle_{(f)} = a_1^\dagger \left(\sqrt{f} a_2^\dagger + \sqrt{1-f} b_2^\dagger \right) |0, 0\rangle_1 |0, 0\rangle_2 \quad (\text{A1})$$

After the BS, shown in Figure 3a, the state will be transformed into

$$\begin{aligned} |1, 1\rangle_{(f)} \mapsto & \frac{\sqrt{f}}{\sqrt{2}} (|2, 0\rangle_1 |0, 0\rangle_2 - |0, 0\rangle_1 |2, 0\rangle_2) \\ & + \frac{\sqrt{1-f}}{2} (|1, 1\rangle_1 |0, 0\rangle_2 - |0, 0\rangle_1 |1, 1\rangle_2) \\ & + \frac{\sqrt{1-f}}{2} (-|1, 0\rangle_1 |0, 1\rangle_2 + |0, 1\rangle_1 |1, 0\rangle_2) \quad (\text{A2}) \end{aligned}$$

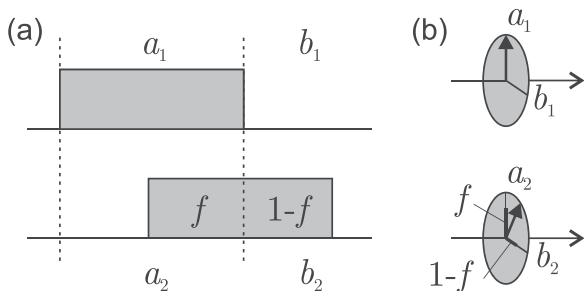


Figure A1. Schematic representation of partially overlapping modes \hat{a} and \hat{b} . The overlap f corresponds to the temporal (a) or polarization (b) degree of freedom.

Further, we assume that the detector D_1 (see Figure 3) does not distinguish between the modes a_1 and b_1 , and the detector D_2 does not distinguish a_2 and b_2 , that is, the detection results are determined by the photon-number operators $\hat{n}_1 = a_1^\dagger a_1 + b_1^\dagger b_1$ and $\hat{n}_2 = a_2^\dagger a_2 + b_2^\dagger b_2$, respectively. Therefore, the first two lines of Equation (A2) correspond to the presence of two photons in one arm of the interferometer, while the third line describes the two photons distributed between the arms yielding coincident counts.

Direct substitution of the state (A2) into the definition of the normalized intensity correlation function (12) yields

$$\bar{g}_2 = \frac{1-f}{2} \quad (\text{A3})$$

for the partially overlapping single-photon inputs of the interferometer.

To calculate the signals and their variances for scaled emulation, it is useful to consider the interference of two partially overlapping PCSs with the scaled amplitudes s_j and s_k at the BS. The resulting mean and mean-squared values of the measured quantities take the following values for a 2-mode probe state $\rho_{\text{PCS}}(s x_j) \otimes \rho_{\text{PCS}}(s x_k)$:

$$I_1(j, k) = I_2(j, k) = A_{jk}, \quad A_{jk} = \eta s^2 \frac{x_j^2 + x_k^2}{2} \quad (\text{A4})$$

$$C_{12}(j, k) = A_{jk}^2 - B_{jk}^2, \quad B_{jk} = \eta s^2 \sqrt{\frac{f}{2}} x_j x_k, \quad (\text{A5})$$

$$I_1^2(j, k) = I_2^2(j, k) = A_{jk}^2 + A_{jk} + B_{jk}^2 \quad (\text{A6})$$

and

$$C_{12}^2(j, k) = A_{jk}^4 + 2A_{jk}^3 + A_{jk}^2 - 2A_{jk}^2 B_{jk}^2 - 2A_{jk} B_{jk}^2 + \frac{3B_{jk}^4}{2} - B_{jk}^2 \quad (\text{A7})$$

According to the emulation protocol, the final expectation value of the emulated quantity X ($X = I_1, I_2$, or C_{12}) equals

$$X = \sum_{j,k} c_j c_k X(j, k) \quad (\text{A8})$$

while its variance can be calculated as

$$\text{Var } X = \sum_{j,k} |c_j| |c_k| X^2(j, k) - X^2 \quad (\text{A9})$$

The numerical results are shown in Figure 4. It is worth noting that the efficiency of the detectors η enters the expressions together with the scaling parameter s as a combination ηs^2 . The expectation values of intensities and the coincidence signal scale as ηs^2 and $(\eta s^2)^2$, respectively, thus ensuring \bar{g}_2 independence of scaling. However, the expressions for the variances of the measured quantities contain terms growing slower with ηs^2 than the main term and vanishing for bright scaled emulation. Figure A2 shows the dependence of the standard deviation of the re-normalized correlation function $2\bar{g}_2$ on the effective scaling parameter ηs^2 . One can see that the effect of scaling with the statistical errors saturates for $\eta s^2 \sim 10$; the remaining noise is caused by random sampling of the probe states rather than by their internal noise.

Appendix B: Optimization of Single-Photon State Representation

Here, we illustrate how one can develop a high-fidelity representation of a single-photon state in terms of the PCSs. For constructing such a representation, we minimize the error defined as

$$d = \sqrt{\sum_{n=0}^{N_{\max}} |\rho_{nn}^{\text{est}} - \rho_{nn}^{\text{true}}|^2} \quad (\text{B1})$$

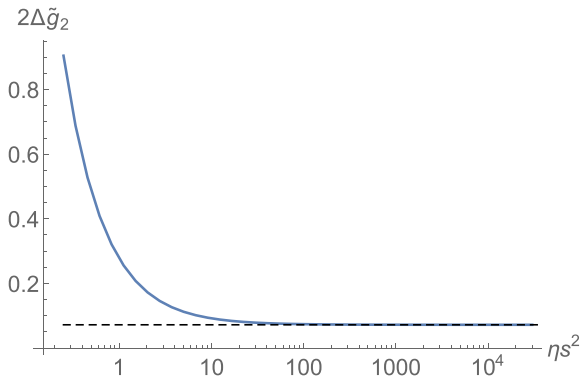


Figure A2. Dependence of the standard deviation of the emulated re-normalized second-order correlation function $2\Delta\tilde{g}_2(\theta)$ on the effective scaling parameter ηs^2 . Dashed horizontal line indicates the asymptotic value of the standard deviation.

where $\rho_{nn}^{est (true)}$ are diagonal elements of the estimated (true) density matrix. We utilize the least-square fitting (LSF) algorithm of the CVX package in MATLAB, and the genetic algorithm (GA) to optimize the emulation. The variables of the optimization problem are the amplitudes of the probe states $|\alpha_k\rangle$, and the decomposition coefficients c_k . The constraint condition is the positivity of the elements of the constructed density matrix. The number of the probe states K was chosen as the minimal one providing a reasonable accuracy of the representation for sufficiently small values of the normalization coefficient C in Equation (4).

As the first example, we assume a uniform distribution for the amplitudes of the coherent states by considering an equidistant linear lattice with the grid distance δ (corresponding to the difference between the amplitude of two adjacent coherent states). Then, the amplitude sequence

is $|\alpha_k\rangle = k\delta$ with $k \in 1 \dots K$. By setting δ as a variable of the GA, we obtain the optimum value of $\delta = 0.305$ for representation of a single-photon state by 8 PCSs. Using the LSF algorithm, the weight coefficients are derived and shown in **Figure B1(a)**. **Figure B1(b)** shows the diagonal terms of the estimated (true) density matrix by gray (red) bars and the inset plot is a zoom-in view of the dashed box. As one can see, $\rho_{11}^{est} \approx 1$ and the rest of the diagonal elements are very small as expected. The error distance is 3.66×10^{-5} , which indicates an accurate emulation. By changing the constraint tolerance in the GA, the accuracy can be further increased if needed. Since the GA is a stochastic algorithm, the results may slightly change at each run.

Next, we set $|\alpha_k\rangle$ as optimized variables in the GA and derive a set of amplitudes with nonuniform distribution in a linear lattice as shown in **Figure B1(c)** as well as their corresponding weights. For this case, the estimated density matrix is illustrated in **Figure B1(d)**, which is well-matched to the true state with the error distance 1.81×10^{-5} .

Generally, noise in PCSs, actually used for emulation, spoils the resulting accuracy. However, the effect can be removed by taking the noise into account initially: when specifying the probe states and constructing the representation (2). One can aim at representing the target state in terms of PCSs with noisy amplitude:

$$\rho_{PCS}(x, \sigma) = \frac{1}{\sqrt{2\pi}\sigma} \int_{-\infty}^{\infty} dy \exp\left(-\frac{(y-x)^2}{2\sigma^2}\right) \rho_{PCS}(|y\rangle) \quad (B2)$$

Numerical results for such representation are shown in **Figure B2**. If the probe states are noisy, an increased number of such states becomes necessary.

Appendix C: Scaled Emulation of Phase Estimation

The state (A2), obtained after the interference of 2 photons at a beam-splitter, is close to the 2-photon NOON-state $(|2\rangle_a|0\rangle_b - |0\rangle_a|2\rangle_b)/\sqrt{2}$

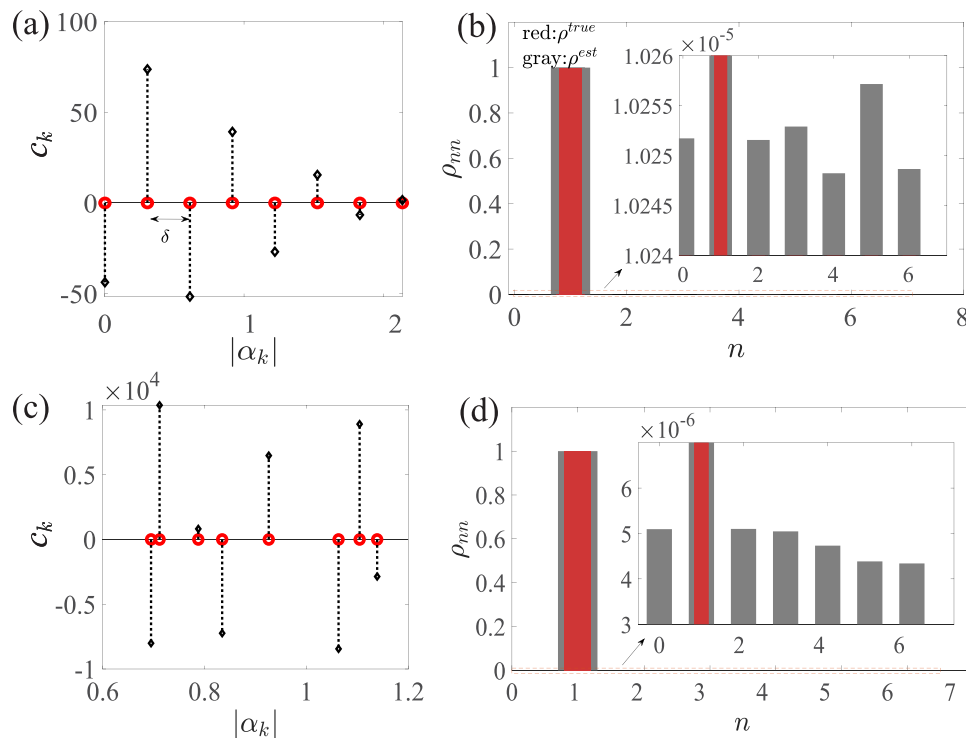


Figure B1. Emulation of a single-photon state by 8 PCSs using (a) an equidistant linear lattice and (c) a nonuniform linear lattice with the corresponding weights c_k . The shown true and emulated density matrices are related to the uniform (b) and nonuniform lattices (d).

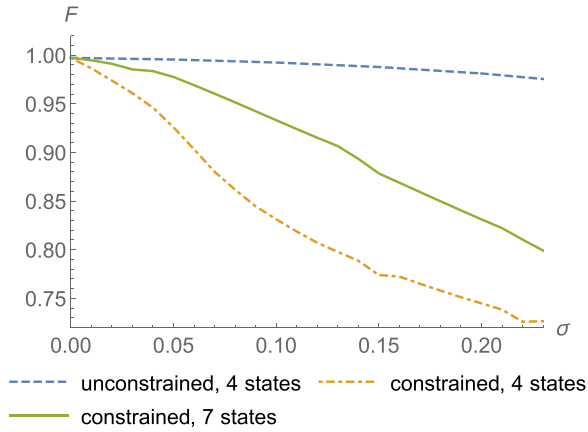


Figure B2. Dependence of the fidelity of single-photon state decomposition (2) in terms of noise PCSs (B2) on the noise amplitude σ for unconstrained optimization with 4 probe states (dashed) and constrained optimization with $C \leq 30$ and 4 (dot-dashed) and 7 (solid) probe states.

and, therefore, can be used for sensitivity enhancement in phase estimation. For the scheme, shown in Figure 5, the normalized coincidence rate takes the following value for interference of a pair of single photons with the overlap f :

$$\tilde{g}_2(\theta) = \frac{1-f}{2} + \frac{1+f}{2} \cos^2 \theta \quad (C1)$$

The expressions for the mean and mean-squared values of the measured observables, similar to Equations (A4)–(A7), take the following form for a 2-mode probe state $\rho_{\text{PCS}}(sx_j) \otimes \rho_{\text{PCS}}(sx_k)$:

$$I_{1,2}(j, k) = D_{jk}^{(\mp)}, \quad D_{jk}^{(\pm)} = \eta s^2 \left(x_j^2 \frac{1 \mp \cos \theta}{2} + x_k^2 \frac{1 \pm \cos \theta}{2} \right) \quad (C2)$$

$$C_{12}(j, k) = D_{jk}^{(+)} D_{jk}^{(-)} - J_{jk}, \quad J_{jk} = \frac{\eta^2 s^4}{2} f x_j^2 x_k^2 \sin \theta \quad (C3)$$

$$I_{1,2}^2(j, k) = \left(D_{jk}^{(\mp)} \right)^2 + D_{jk}^{(\mp)} + J_{jk} \quad (C4)$$

and

$$C_{12}^2(j, k) = D_{jk}^{(+)} D_{jk}^{(-)} \left(1 + D_{jk}^{(+)} \right) \left(1 + D_{jk}^{(-)} \right) + \left[\left(D_{jk}^{(+)} \right)^2 + \left(D_{jk}^{(-)} \right)^2 - 4 D_{jk}^{(+)} D_{jk}^{(-)} - D_{jk}^{(+)} - D_{jk}^{(-)} - 1 \right] J_{jk} + \frac{3 J_{jk}^2}{2} \quad (C5)$$

The results, calculated according to the derived expression, are shown in Figure 6 for $N = 10^7$ repetitions.

Appendix D: Expressions for Emulation of “Collapses” and “Revivals”

The dynamics of atom-field state yielding “collapses” and “revivals” is described by Jaynes-Cummings Hamiltonian (38). In the initial state, the atom is assumed to be in the lower state $|-\rangle$, while the field mode is in certain state (a coherent one, a PCS, or a sub-Poissonian state)

$$\rho = \sum_{m,n=0}^{\infty} \rho_{mn} |m\rangle \langle n| \quad (D1)$$

The solution of Schrödinger equation with the Hamiltonian (38) and the initial condition (D1) is

$$\rho_{\text{atom+field}}(t) = \sum_{mn=0}^{\infty} \rho_{mn} |\Psi_m(t)\rangle \langle \Psi_n(t)| \quad (D2)$$

where

$$|\Psi_k(t)\rangle = |k\rangle |-\rangle \cos \left[\frac{\Omega \sqrt{nt}}{2} \right] - i |k-1\rangle |+\rangle \sin \left[\frac{\Omega \sqrt{nt}}{2} \right] \quad (D3)$$

is the solution for the initial k -photon state of the field mode. Therefore, the population inversion is described by Equation (39) with $p(n) = \rho_{nn}$ being the diagonal part of the density matrix of the initial field mode state.

For the initial coherent state $\rho = |\alpha\rangle \langle \alpha|$ (blue line in Figure 10a) one has $p(n) = |\alpha|^{2n} e^{-|\alpha|^2} / n!$ and

$$P(t) \equiv P(t; |\alpha\rangle) = \sum_{n=1}^{\infty} \frac{|\alpha|^{2n}}{n!} e^{-|\alpha|^2} \sin^2 \left[\frac{\Omega \sqrt{nt}}{2} \right] \quad (D4)$$

For the initial sub-Poissonian state (orange line in Figure 10b) the expression (26) was substituted into Equation (39) for calculation of $P(t)$.

According to linearity of quantum dynamics, the population inversion for the emulated experiment (blue line in Figure 10b) can be calculated in the following way:

$$P(t) = \sum_k c_k P(t; |\alpha_k\rangle) \quad (D5)$$

where the population inversion for PCSs is provided by Equation (D4).

Here, one should notice that in the resonant Jaynes-Cummings model, for a very large number of photons and/or long evolution times and low loss, the rotating wave approximation eventually breaks down leading to deviations from behaviour described by Equation (39).^[78,79]

Acknowledgements

All the authors acknowledge support from the NATO project NATO 560 SPS-G5860. Also, D.M., A. M. and S. V. gratefully acknowledge support from the BRFFR Project No. F22B-008.

Conflict of Interest

The authors declare no conflict of interest.

Data Availability Statement

The data that support the findings of this study are available from the corresponding author upon reasonable request.

Keywords

bright nonclassical states, emulation, quantum measurements

Received: March 9, 2023
Revised: May 22, 2023
Published online:

- [1] L. Davidovich, *Rev. Mod. Phys.* **1996**, 68, 127.
- [2] M. Walschaers, *PRX Quantum* **2021**, 2, 030204.
- [3] N. Biagi, S. Francesconi, A. Zavatta, M. Bellini, *Prog. Quantum Electron.* **2022**, 84, 100414.
- [4] D. Achilles, C. Silberhorn, C. Sliwa, K. Banaszek, I. A. Walmsley, M. J. Fitch, B. C. Jacobs, T. B. Pittman, J. D. Franson, *J. Mod. Opt.* **2004**, 51, 1499.
- [5] B. Kardynal, Z. Yuan, A. Shields, *Nat. Photonics* **2008**, 2, 425.
- [6] A. E. Lita, A. J. Miller, S. W. Nam, *Opt. Express* **2008**, 16, 3032.
- [7] F. Mattioli, Z. Zhou, A. Gaggero, R. Gaudio, S. Jahanmirinejad, D. Sahin, F. Marsili, R. Leoni, A. Fiore, *Supercond. Sci. Technol.* **2015**, 28, 104001.
- [8] Y. S. Teo, H. Jeong, J. Řeháček, Z. Hradil, L. L. Sánchez-Soto, C. Silberhorn, *Quantum Reports* **2019**, 1, 162.
- [9] M. Cramer, M. B. Plenio, S. T. Flammia, R. Somma, D. Gross, S. D. Bartlett, O. Landon-Cardinal, D. Poulin, Y.-K. Liu, *Nat. Commun.* **2010**, 1, 149.
- [10] G. Tóth, W. Wieczorek, D. Gross, R. Krischek, C. Schwemmer, H. Weinfurter, *Phys. Rev. Lett.* **2010**, 105, 250403.
- [11] B. P. Lanyon, C. Maier, M. Holzäpfel, T. Baumgratz, C. Hempel, P. Jurcevic, I. Dhand, A. S. Buyskikh, A. J. Daley, M. Cramer, M. B. Plenio, R. Blatt, C. F. Roos, *Nat. Phys.* **2017**, 13, 1158.
- [12] H.-Y. Huang, R. Kueng, J. Preskill, *Nat. Phys.* **2020**, 16, 1050.
- [13] S. Aaronson, *SIAM J. Comput.* **2019**, 49, STOC18.
- [14] U. L. Andersen, T. Gehring, C. Marquardt, G. Leuchs, *Phys. Scr.* **2016**, 91, 053001.
- [15] C. Weedbrook, S. Pirandola, R. García-Patrón, N. J. Cerf, T. C. Ralph, J. H. Shapiro, S. Lloyd, *Rev. Mod. Phys.* **2012**, 84, 621.
- [16] M. Reck, A. Zeilinger, H. J. Bernstein, P. Bertani, *Phys. Rev. Lett.* **1994**, 73, 58.
- [17] A. Windhager, M. Suda, C. Pacher, M. Peev, A. Poppe, *Opt. Commun.* **2011**, 284, 1907.
- [18] A. I. Lvovsky, S. A. Babichev, *Phys. Rev. A* **2002**, 66, 011801.
- [19] A. Zavatta, S. Viciani, M. Bellini, *Science* **2004**, 306, 660.
- [20] J. Wenger, R. Tualle-Brouri, P. Grangier, *Phys. Rev. Lett.* **2004**, 92, 153601.
- [21] A. Zavatta, V. Parigi, M. S. Kim, M. Bellini, *New J. Phys.* **2008**, 10, 123006.
- [22] O. Magaña-Loaiza, R. J. León-Montiel, A. Perez-Leija, A. U'Ren, C. You, K. Busch, A. Lita, S. Nam, R. Mirin, T. Gerrits, *npj Quant. Inf.* **2019**, 5, 80.
- [23] D. Su, C. R. Myers, K. K. Sabapathy, *Phys. Rev. A* **2019**, 100, 052301.
- [24] E. Flurin, N. Roch, F. Mallet, M. H. Devoret, B. Huard, *Phys. Rev. Lett.* **2012**, 109, 183901.
- [25] X. Gu, A. F. Kockum, A. Miranowicz, Y.-x. Liu, F. Nori, *Phys. Rep.* **2017**, 718, 1.
- [26] C. Macklin, K. O'Brien, D. Hover, M. E. Schwartz, V. Bolkhovskiy, X. Zhang, W. D. Oliver, I. Siddiqi, *Science* **2015**, 350, 307.
- [27] O. Kyriienko, A. S. Sørensen, *Phys. Rev. Lett.* **2016**, 117, 140503.
- [28] K. Inomata, Z. Lin, K. Koshino, W. Oliver, J.-S. Tsai, T. Yamamoto, Y. Nakamura, *Nat. Commun.* **2016**, 7, 12303.
- [29] J. H. Shapiro, *Phys. Rev. A* **2008**, 78, 061802.
- [30] J. Zhao, J. Dai, B. Braverman, X.-C. Zhang, R. W. Boyd, *Optica* **2021**, 8, 1176.
- [31] A. Mikhalychev, Y. S. Teo, H. Jeong, A. Stefanov, D. Mogilevtsev, *Phys. Rev. A* **2022**, 105, 052206.
- [32] P. F. Góra, C. Jedrzejek, *Phys. Rev. A* **1993**, 48, 3291.
- [33] E. Jaynes, F. Cummings, *Proc. IEEE* **1963**, 51, 89.
- [34] C. K. Hong, Z. Y. Ou, L. Mandel, *Phys. Rev. Lett.* **1987**, 59, 2044.
- [35] H. Lee, P. Kok, J. P. Dowling, *J. Mod. Opt.* **2002**, 49, 2325.
- [36] J. H. Eberly, N. B. Narozhny, J. J. Sanchez-Mondragon, *Phys. Rev. Lett.* **1980**, 44, 1323.
- [37] M. V. Satyanarayana, P. Rice, R. Vyas, H. J. Carmichael, *JOSA B* **1989**, 6, 228.
- [38] M. O. Scully, M. S. Zubairy, *Quantum Optics*, Cambridge University Press, Cambridge **1997**.
- [39] L. Mandel, *Phys. Scr.* **1986**, 1986, 34.
- [40] C. H. Bennett, *Phys. Rev. Lett.* **1992**, 68, 3121.
- [41] D. Horoshko, M. Eskandari, S. Kilin, *Phys. Lett. A* **2019**, 383, 1728.
- [42] D. Gottesman, I. Chuang, *arXiv preprint quant-ph/0105032*, **2001**.
- [43] P. J. Clarke, R. J. Collins, V. Dunjko, E. Andersson, J. Jeffers, G. S. Buller, *Nat. Commun.* **2012**, 3, 1174.
- [44] P. D. Drummond, B. Opanchuk, L. Rosales-Zárate, M. D. Reid, *Phys. Scr.* **2014**, 2014, 014009.
- [45] L. Rosales-Zárate, B. Opanchuk, P. D. Drummond, M. D. Reid, *Phys. Rev. A* **2014**, 90, 022109.
- [46] H. J. Korsch, C. Müller, H. Wiescher, *J. Phys. A: Math. Gen.* **1997**, 30, L677.
- [47] U. Chabaud, D. Markham, F. Grosshans, *Phys. Rev. Lett.* **2020**, 124, 063605.
- [48] J. Řeháček, D. Mogilevtsev, Z. Hradil, *Phys. Rev. Lett.* **2010**, 105, 010402.
- [49] D. Mogilevtsev, A. Ignatenko, A. Maloshtan, B. Stoklasa, J. Rehacek, Z. Hradil, *New J. Phys.* **2013**, 15, 025038.
- [50] L. Motka, B. Stoklasa, J. Rehacek, Z. Hradil, V. Karasek, D. Mogilevtsev, G. Harder, C. Silberhorn, L. L. Sánchez-Soto, *Phys. Rev. A* **2014**, 89, 054102.
- [51] A. Mikhalychev, D. Mogilevtsev, Y. S. Teo, J. Řeháček, Z. Hradil, *Phys. Rev. A* **2015**, 92, 052106.
- [52] V. Reut, A. Mikhalychev, D. Mogilevtsev, *Phys. Rev. A* **2017**, 95, 012123.
- [53] L. Motka, M. Paúr, J. Řeháček, Z. Hradil, L. L. Sánchez-Soto, *New J. Phys.* **2021**, 23, 073033.
- [54] J. G. Rarity, P. R. Tapster, R. Loudon, *J. Opt. B: Quantum Semiclassical Opt.* **2005**, 7, S171.
- [55] C. Lang, C. Eichler, L. Steffen, J. Fink, M. Woolley, A. Blais, A. Wallraff, *Nat. Phys.* **2013**, 9, 345.
- [56] D. Bozyigit, C. Lang, L. Steffen, J. Fink, C. Eichler, M. Baur, R. Bianchetti, P. Leek, S. Filipp, M. Silva, A. Blais, A. Wallraff, *Nat. Phys.* **2011**, 7, 154.
- [57] D. B. Horoshko, S. De Bièvre, G. Patera, M. I. Kolobov, *Phys. Rev. A* **2019**, 100, 053831.
- [58] V. Giovannetti, S. Lloyd, L. Maccone, *Science* **2004**, 306, 1330.
- [59] R. Demkowicz-Dobrzanski, J. J. Kolodynski, M. Guta, *Nat. Commun.* **2012**, 3, 1063.
- [60] J. P. Dowling, *Phys. Rev. A* **1998**, 57, 4736.
- [61] H. Barnum, C. M. Caves, C. A. Fuchs, R. Jozsa, B. Schumacher, *Phys. Rev. Lett.* **1996**, 76, 2818.
- [62] M. A. Nielsen, *arXiv preprint quant-ph/9606012*, **1996**.
- [63] R. J. Glauber, *Phys. Rev.* **1963**, 131, 2766.
- [64] L. Mandel, *Opt. Lett.* **1979**, 4, 205.
- [65] G. Rempe, H. Walther, N. Klein, *Phys. Rev. Lett.* **1987**, 58, 353.
- [66] Y. Kaluzny, P. Goy, M. Gross, J. M. Raimond, S. Haroche, *Phys. Rev. Lett.* **1983**, 51, 1175.
- [67] A. Boca, R. Miller, K. M. Birnbaum, A. D. Boozer, J. McKeever, H. J. Kimble, *Phys. Rev. Lett.* **2004**, 93, 233603.
- [68] T. Yoshie, A. Scherer, J. Hendrickson, G. Khitrova, H. M. Gibbs, G. Rupper, C. Ell, O. B. Shchekin, D. G. Deppe, *Nature* **2004**, 432, 200.
- [69] J. McKeever, A. Boca, A. D. Boozer, J. R. Buck, H. J. Kimble, *Nature* **2003**, 425, 268.
- [70] K. Hennessy, A. Badolato, M. Winger, D. Gerace, M. Atatüre, S. Gulde, S. Fält, A. EL Hu, A. Imamoglu, *Nature* **2007**, 445, 896.
- [71] S. Y. Kilin, T. B. Krinitskaya, *JOSA B* **1991**, 8, 2289.
- [72] A. B. Mikhalychev, S. V. Vlasenko, S. Y. Kilin, *Phys. Rev. A* **2022**, 105, 063723.

- [73] S. Y. Kilin, T. B. Karlovich, *J. Exp. Theor. Phys.* **2002**, 95, 805.
- [74] S. Y. Kilin, A. B. Mikhalychev, *Phys. Rev. A* **2012**, 85, 063817.
- [75] S. Y. Kilin, A. B. Mikhalychev, *Phys. Scr.* **2014**, 2014, 014021.
- [76] V. P. Stefanov, S. Y. Kilin, *Nonlinear Phenom. Complex Syst.* **2019**, 22, 64.
- [77] D. B. Horoshko, C.-S. Yu, S. Y. Kilin, *JOSA B* **2021**, 38, 3088.
- [78] I. D. Feranchuk, A. V. Leonov, O. D. Skoromnik, *J. Phys. A: Math. Theor.* **2016**, 49, 454001.
- [79] I. Feranchuk, A. Leonov, *Phys. Lett. A* **2011**, 375, 385.